Estimation of Optimal Range for Shape From Focus in Microscopic System

Hulya Dogan*‡, Elif Baykal Kablan*, Murat Ekinci*, Mustafa Emre Ercin**, Safak Ersoz**

* Department of Computer Engineering, Faculty of Engineering, Karadeniz Technical University, Trabzon, Turkey

** Department of Pathology, Faculty of Medicine, Karadeniz Technical University, Trabzon, Turkey

(hulya, ebaykal, ekinci, drmustafaemreercin, sersoz@ktu.edu.tr)

‡Corresponding Author; Hulya DOGAN, Karadeniz Technical University, Tel: +90 462 377 4384, hulya@ktu.edu.tr

Received: 06.01.2021 Accepted: 29.03.2021

Abstract- Shape From Focus (SFF) is one of the most preferred approaches in microscopic systems to reconstruct the 3D shape of the specimen. Classical approach generates a 3D shape using the 2D image sequence with the same field of perspective and different focused regions. In order to scan the specimen in traditional SFF approaches, the microscope platform is moved along the specified range, which is randomly defined between the begin and end locations on the Z axis. A certain amount of 2D image sequence with the same field of perspective and different focused regions are acquired in limited movements between these locations. However, the range and amount of 2D image sequence are effective to extract the entire 3D structure of the specimen, they must be optimized for the type of the examined specimen and magnification objective. In this study, a novel SFF approach is improved to scan the whole 3D structure of the specimen by estimating the optimal range between the begin and end locations of microscope platform. Unlike previous approaches, problems such as random amount of 2D image sequence with the same field of perspective and different focused regions, random determination of the range between the begin and end locations and the occurrence of outliers and noise around the 3D shape are solved in the proposed approach. Our experiments are performed on data sets collected from the light microscopy using specimen prepared for cytopathological examination. Qualitative and quantitative results demonstrate that better performance is achieved by our suggested SFF approach.

Keywords Focus measurement operator, Shape from focus, 3D shape reconstruction, Cytopathological examination.

1. Introduction

Cytopathological examination is described as the analysis of cells in the specimen under the microscopic system. This is accomplished with eye - hand coordination by the pathologist, and used to determine what cells look like, and how they form. The whole structure of the specimen cannot be fully examined by the pathologist, as the specimen region has lost one dimension from the real - world scene (3D) to the image plane (2D) projection. 3D shape reconstruction of the specimen provides the structure of the cell more visible, and allows the pathologist detect the location and size of the cells in the specimen more reliably. It is derived from literature studies that 3D shape reconstruction is one of the areas that have been actively studied in the microscopic system for many years and significantly improves the performance of cell segmentation and detection methods. The equipment which removes the specimen's 3D shape in the microscopic system is categorized into two parts, passive and active. Passive equipment does not require any additional device to measure the distance between the specimen and magnification objective, while the active equipment uses infrared or ultrasonic waves. For 3D shape reconstruction of the specimen in the microscopic systems, approaches in the literature can be classified into two groups, photometric and geometrical [1]. Pixel focus values in the specimen region are utilized to remove the specimen's 3D shape in

photometric approaches where a single-lens camera is used. Shape From Focus (SFF) can be given as an example of these approaches. In geometrical approaches where two or three ocular cameras are located, information about the specimen region structure and the camera's internal and external parameters are used. Stereo imaging can be given as an example of these approaches.

3D shape reconstruction of the specimen is one of the most studied areas in the microscopic system. Recent literature review proves that SFF that requires a 2D image sequence with the same field of perspective and different focused regions is generally applied to reconstruct the 3D shape of the specimen in the microscopic systems [2,3]. In the SFF approach, the focusing values of the pixels are fundamental keys for generating the 3D shape of the specimen. The classical version of this approach, which does not require any physical contact between the displayed specimen area and the optical system, comprises of three critical phases: (1) Creating 2D image sequence with the same field of perspective and different focused regions. In the microscopic system, this image sequence is created with an extended depth of focus. This system has a restricted depth of focus, which is widely measured in microns. When the size of the specimen analysed in the microscopic system is greater than this distance, only some parts of the specimen appear focused. In order to create a 2D image sequence with the same field of perspective and different focused regions, all regions of the specimen are scanned along the depth of focus by moving the microscope platform with limited movements on the Z axis. (2) Computing focus measure sequence. In the microscopic system, focus measure sequence consisting of the focusing information of each pixel in the 2D image sequence with the same field of perspective and different focused regions is obtained. Researchers have suggested various focus measurement operators to calculate the pixel's focus degree, and categorize these focus measurement operators into six subgroups [2]; (1) Gradient - based (Tenengrad [2], Gaussian Derivative [4], Tenengrad Variance [2], Gradient Energy [5], 3D Gradient [6], Squared Gradient [2] and Thresholded Absolute Gradient [2]), (2) Laplacian - based (Laplacian in 3D [7], Variance of Laplacian [8], Energy of Laplacian [6], Multidirectional Modified Laplacian [9], Modified Laplacian [10]), (3) Statistics - based (Histogram Range [2], Eigen Values [11], Normalized Variance [2], Chebyshev Moments [12], Histogram Entropy [2], Local Variance [8], Modified Variance [2] and Variance [2]), (4) Discrete Cosine Transform (DCT) - based (Modified DCT [13], DCT Reduced Energy Ratio [14] and DCT Energy Ratio [15]), (5) Wavelet - based (3D Wavelet Transform [16], Wavelet Coefficient Ratio, Wavelet Coefficient Variance and Wavelet Coefficient Sum [17]), and (6) Other operators (Brenner [2], Helmli and Scherer [18], Autocorrelation [2], Absolute Central Moment [19], Image Curvature [18], Spatial Frequency [2], Image Contrast [20], Local Binary Pattern [21], Curvelet Coefficients Ratio [22], Gabor Features [23], 2D Steerable and 3D Steerable Filters [24]. (3) Selecting pixel with maximum focus degree. In order to reconstruct the specimen's 3D shape, which includes the point distances between the displayed specimen area and the optical system, this phase determines the pixels with the highest focus measure in the focus measure sequence.

In the literature, Nayar first proposed the basic phases of the classical SFF approach [10], and studies for the SFF approach in the microscopic system can be organized as follows: (1) the proposal of a novel focus measurement operator: in the first category, the researchers have suggested a novel algorithm to extract measures about the focusing information of the pixels in the 2D image sequence [2, 4-24]. (2) Comparative analysis of the suggested focus measurement operators under different scenarios such as window size, image noise, density and distortion [2]. (3) Improvement of the 3D shape reconstruction created with the classical SFF approach: in this category, researchers proposed a pre- or post-processing algorithm to generate 3D shape reconstruction with higher accuracy and lower noise. Examples for these algorithms are reliability measure [25], adaptive window selection [26], mathematical solution for window size selection [27], spatial consistency model [28], adaptive smoothness constraint based on the Modified Laplacian calculation [29], focus profile modelling [30]. (4) Analysis of the sampling step size between 2D images with the same field of perspective and different focused regions: In the fourth category, researchers have analysed the sampling step size which is another critical factor affecting SFF approaches. Muhammad et al. [31] formulated inter-frame distance (sampling size) for SFF systems.

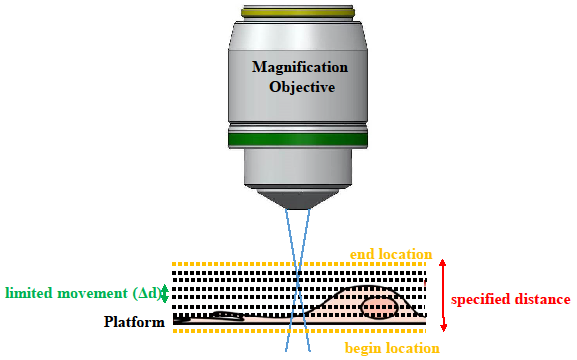

Fig. 1. Scanning of specimen on the Z axis for the first phase (Creating 2D image sequence with the same field of perspective and different focused regions) of SFF.

In the classical SFF approach for the microscopic system, the specimen is scanned by moving the microscope platform along the specified range that is randomly defined between the begin and end locations on the Z axis. As shown in Fig.1, a certain amount of 2D image sequence with the same field of perspective and different focused regions are acquired in limited movements (Δd) between these locations for the first phase (Creating 2D image sequence with the same field of perspective and different focused regions) of SFF. Moreover, this amount of 2D image sequence with the same field of perspective and different focused regions is not altered depending on the microscope objective and specimen type. However, the range between the begin and end locations on the Z - axis and the amount of 2D image sequence with the same field of perspective and different focused regions are seen to be effective in extracting the

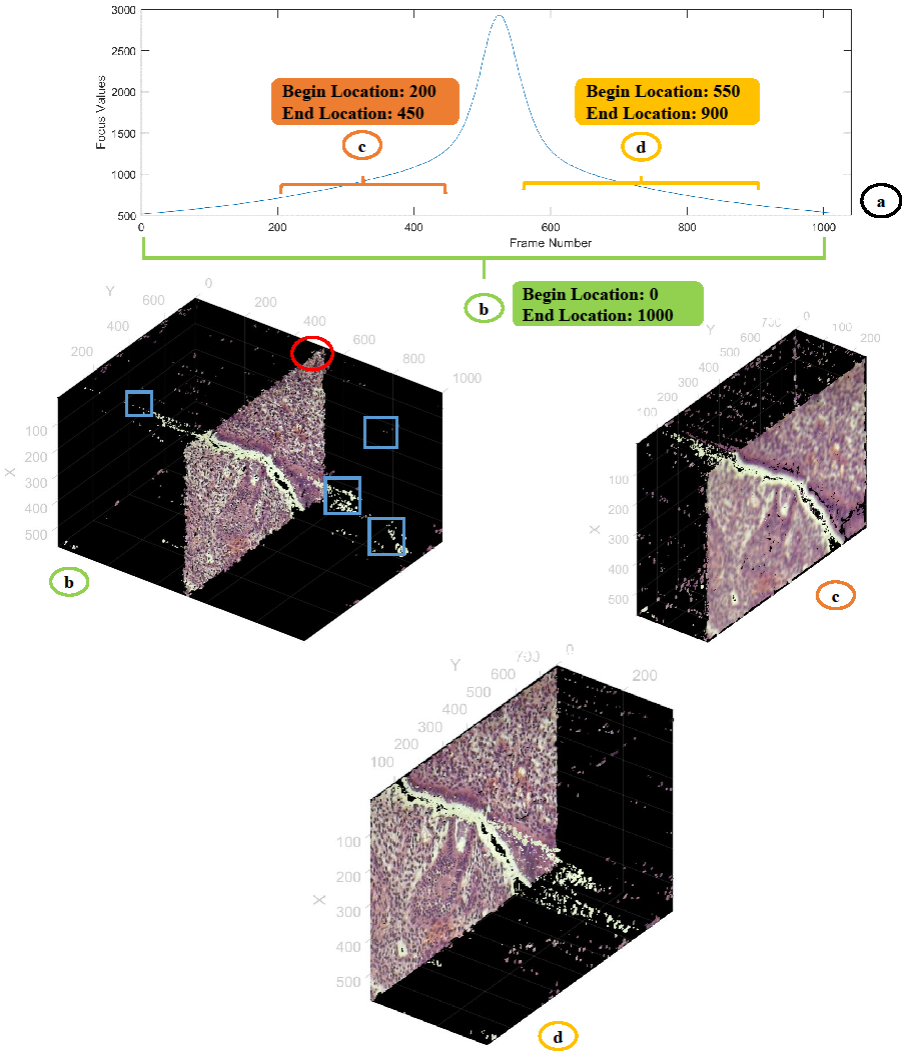

Fig. 2. (a) Focus measures of 2D image sequence with the same field of perspective and different focused regions, (b) 3D shape generated using all 2D images, (c) 3D shape generated using 2D images between begin (200) and end (450) locations, (d) 3D shape generated using 2D images between begin (550) and end (900) locations.

specimen's complete 3D structure. Although various studies for the SFF approach in the microscopic system, less attention was given to the amount of 2D image sequence with the same field of perspective and different focused regions or the range between the begin and end locations on the Z - axis. In order to denote the effectiveness of the amount of 2D images and the range for extraction of specimen's complete 3D structure with lower variations and outliers, a sequence of 1000 2D images with the same field of perspective and different focused regions are taken by moving the platform on the Z axis in 0.0125 micrometres steps. In this image acquisition process, the begin and end locations are defined randomly. Fig.2.a gives focus measures of the 2D image sequence with the same field of perspective and different focused regions. The SFF approach, in which all 2D images in Fig.2.a are used generates a 3D shape as shown in Fig.2.b. As stated in the red circle, the 3D structure of this specimen extends over 450 and 550 indices on the Z axis. If the range between the begin and end locations is wide, a huge amount of 2D images that are out of the specimen's 3D shape are needlessly used and outliers and variations happen around the specimen's actual 3D shape as shown in the blue rectangles. In addition, this procedure needs an enormous quantity of time and energy in computation. The other two 3D shapes are reconstructed with specific begin and end locations determined randomly on this sequence to demonstrate that the begin and end locations are crucial for acquiring all focus information in the specimen. A 2D image sequence is acquired from the begin location (200) to the end location (450) for the 3D shape shown in Fig.2.c. Moreover, the 3D shape shown in Fig.2.d is generated using 350 2D images between the begin (550) and end (900) locations. The blue rectangles in Fig.2.c and d prove that the random range and reduction of the amount of 2D images cause noisy and erroneous 3D shapes. It is obvious that when the entire specimen is not searched on the Z axis, image focusing information cannot be fully extracted.

This paper has developed a novel SFF approach in which the optimal range is estimated in the microscopic system. Unlike previous approaches, problems such as random amount of 2D image sequence with the same field of perspective and

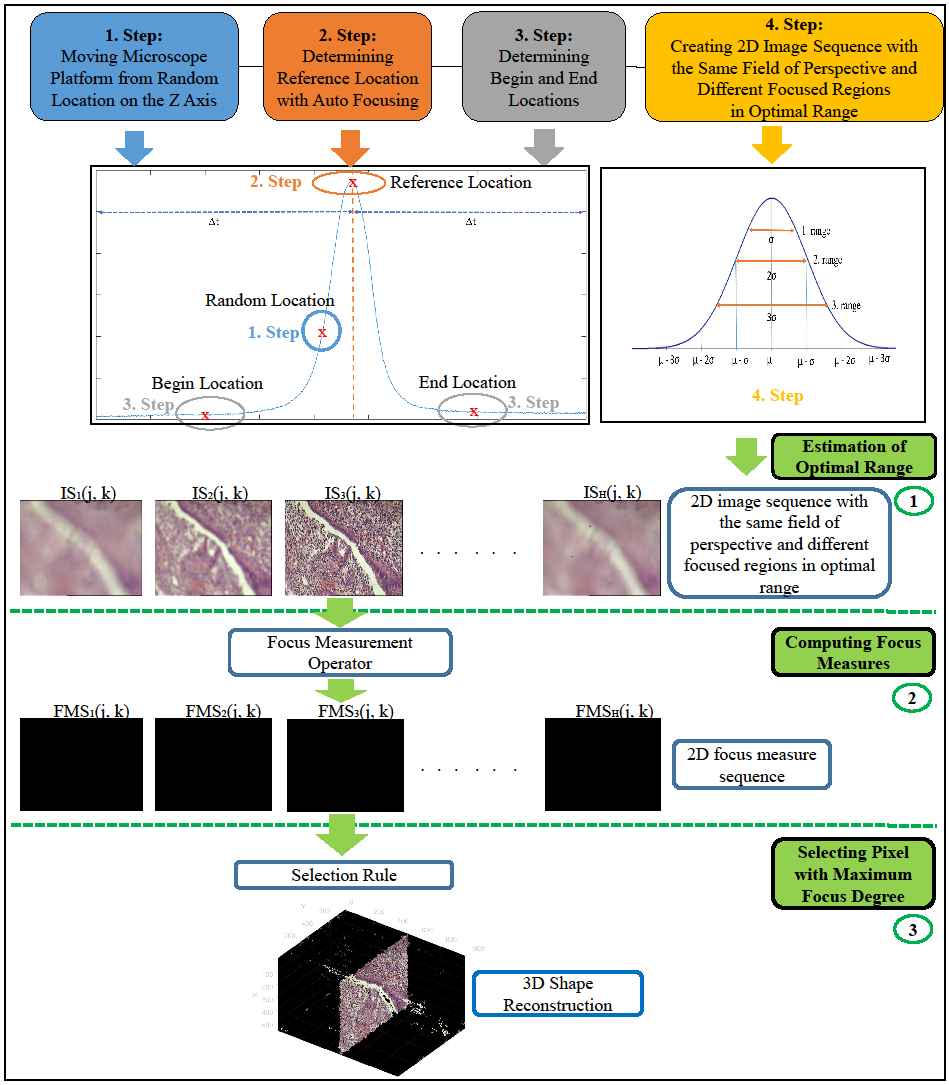

Fig. 3. Primary phases of proposed SFF approach; (1) Estimation of Optimal Range, (2) Computing Focus Measures and (3) Selecting Pixel with Maximum Focus Degree.

different focused regions, random determination of the range between the begin and end locations and the occurrence of outliers and noise around the 3D shape are solved in the proposed approach.

The major contributions of the recommended SFF approach are summarized as follows:

- Regardless of the type of the examined specimen and the microscope objective, the total amount of 2D image sequence with the same field of perspective and different focused regions is optimized.
- The optimal range between the begin and end locations is estimated by formulating the focus measures of 2D images with a specific mathematical model.
- The removal of the entire 3D structure of the specimen on the Z axis is guaranteed.
- Although the recommended SFF approach is designed for cytopathologic examination in the light microscope system, it can be adopted easily to other microscope types (confocal, stereo and laser) with different specimen.
- A novel motorized microscope system with a cheap hardware in price is designed.

2. Methodology

Our novel SFF approach, which guarantees the entire 3D structure of the specimen is extracted by estimating the optimal range between the begin and end locations on the Z axis, is described in this section. As shown in Fig.3, the proposed approach is carried out in three primary phases; estimation of optimal range, computing focus measures and selecting pixel with maximum focus degree.

2.1. Estimation of Optimal Range

In the first phase of the suggested SFF approach, the ideal range is estimated and the specimen's entire 3D structure is scanned on the Z axis in order to create the 3D image with more valuable data and optimal focusing. This phase consists

of four main steps as shown in Fig.3, and the steps are summarized as follows:

1. Moving Microscope Platform from Random Location on the Z Axis

Light microscopic systems generally have a limited depth of focus, measured in micron units. In cases where the size of the specimen scanned in the light microscope for cytopathological examination is larger than the depth of focus, only the part at this depth appears to be focused. Therefore, some regions of the analysed specimen are blurred. In this step, the microscope platform is moved starting from the random location on the Z axis (optical direction) to create a sequence containing 2D images with the same field of perspective and different focused regions.

2. Determining Reference Location with Auto Focusing

From the focus measures of the 2D image sequence with the same field of perspective in Fig.3.a and the 3D shape generated using these 2D images in Fig.3.b, it is understood that the entire 3D structure of the specimen extends on the 2D image with the most focusing information. Moreover, 2D images that are more knowledgeable in terms of focusing appear close to 2D images with the highest focus measure. In order to scan the specimen's entire 3D structure on the Z axis and extract all information in terms of focusing, it should be guaranteed that the 2D images with the highest focus measure and the nearest locations are estimated. For this purpose, the proposed study considers the 2D image with the highest focus measure as the reference location. As mentioned in the previous step, the microscope platform is moved starting from any random location on the Z axis, and the reference location is determined by performing the Auto-Focusing.

The operation steps applied in the suggested Auto-Focusing process are explained as follows:

- The microscope platform is moved by step motor control on the Z axis to acquire a sequence including a fixed number of 2D images with the same field of perspective and different focused regions (in different vertical locations).
- The auto - focusing function is performed to calculate the focus measures of the 2D image sequence.
- Probability density function (pdf) of the 2D image sequence is created by the focus measures.
- The highest measure of pdf is selected and the operation steps are performed until the difference between the highest measures of pdfs is negative.

3. Determining Begin and End Locations

Scanning on the Z axis starts from a random location to create a 2D image sequence with the same field of perspective and different focused regions. Therefore, it cannot be guaranteed to scan the specimen's entire 3D structure that is effective in SFF approaches. As shown in Fig.3, microscope platform is moved in the opposite direction after the Auto-Focusing process to determine the begin location. As given in Eq. (1), the begin location (x_j) is calculated by comparing the difference of the slopes between 2D image locations during the platform movement with a certain threshold value (φ).

$$\left| \frac{fm_j - fm_{j+1}}{x_j - x_{j+1}} - \frac{fm_{j+1} - fm_{j+2}}{x_{j+1} - x_{j+2}} \right| \leq \varphi \quad (1)$$

where x_j, x_{j+1} and x_{j+2} represent the indices of 2D images with the same field of perspective and different focused regions and fm_j, fm_{j+1} and fm_{j+2} indicate the focus measures of 2D images with x_j, x_{j+1} and x_{j+2} locations. In order to determine the end location, the distance (Δt) from the begin location to end location is used as shown in Fig.3. By moving the microscope platform from the begin location to the end location, a 2D image sequence containing the specimen's entire 3D structure on the Z axis is acquired.

4. Creating 2D Image Sequence with the Same Field of Perspective and Different Focused Regions in Optimal Range

The last step defines the ranges with different distances (σ - 2σ - 3σ) on the 2D image sequence (between the begin and end locations). A specific mathematical model based on Gaussian distribution is designed in order to select these ranges regardless of the types of specimen, camera and magnification objective. In the Gaussian Distribution, the focus measures of the 2D image sequence created in the previous step are modelled by taking the reference location as the mean (μ). The designed Gaussian Distribution is in Eq. (2).

$$f(x) = \frac{1}{\sigma\sqrt{2\pi}} e^{-\frac{(x-\mu)^2}{2\sigma^2}} \quad (2)$$

$$\mu = \frac{\sum_{i=1} x_i y_i}{\sum_{i=1} y_i} \qquad \sigma = \sqrt{\sum_{i=1} (x_i - \mu)^2 \frac{y_i}{\sum_{i=1} y_i}}$$

where σ and μ represent standard deviation and mean (reference location) of the focus measures of the 2D image sequence, fm_j is the focus measure of the 2D image on the x_j index.

2.2. Computing Focus Measures

In the second phase of the proposed SFF approach, the focus measures of the pixels in the 2D image sequence with the same field of perspective and different focused regions is computed. In order to create 2D focus measure sequence ($FMS_1(j,k)$,$FMS_2(j,k)$...,$FMS_H(j,k)$) consisting of the focusing information of each pixel in the 2D image sequence, 10 focus measurement operators (Tenengrad [2], Gradient Energy [5], Multidirectional Modified Laplacian [9], Modified Laplacian [10], Variance [2], DCT Energy Ratio [15], 3D Wavelet Transform [16], Wavelet Coefficient Ratio [17], Curvelet Coefficients Ratio [22], 3D Steerable Filters

[24]) selected from different six subgroups are used in this study.

2.3. Selecting Pixel with Maximum Focus Degree

In the third phase of the suggested SFF approach, selection rule is applied in each pixel location in the 2D image sequence in order to reconstruct the specimen's 3D shape, which includes the point distances between the displayed specimen area and the optical system.

3. Experiments and Discussion

3.1. Motorized Microscope System

A novel motorized microscope system is developed in this study, which can automatically analyze the specimen along the X - Y - Z axes and create real 2D microscope images with the same field of perspective and different focused regions are created. Our novel motorized system consists of several materials: a digital microscope CCD camera, a light microscope, a PC with Intel Core i7 CPU, 8 GB RAM and Windows 10 operating system, three step motors which can move the microscope platform along the X - Y - Z axes, a step motor control circuit which provides data transfer between three step motors and PC, a monitor.

3.2. Experiments for Removal of Entire 3D Structure of Specimen on the Z axis

This study aims to demonstrate that standard deviation (SD) of pdf on the 2D image sequence, reference location index (RLI) and the amount of 2D image sequence (AIS) vary with the magnification objective and the displayed specimen region. Therefore, a total of six test sequences given in Table 1 are created using different magnification objectives (10X - 20X - 40X) and the displayed specimen regions. The movement of the microscope platform starts from the random location to acquire these test sequences, consisting of 2D images with the same field of perspective and different focused regions. The reference location is determined by applying the Auto - focusing process. This process is generated using the Variance auto - focusing function in two different displayed specimen regions for each magnification objective (10X - 20X - 40X). In the third step (Determining Begin and End Locations), Manual Trial and Error determines that the threshold value (φ) is 0.01 for all magnification objectives. After determining the end location, the test sequence is completed and the removal of the entire 3D structure of the specimen on the Z axis is guaranteed. As seen in Table 1, the test sequences including different SD, RLI and AIS values are obtained for the magnification objectives 10X (Test Sequences - 1 and 2) and 40X (Test Sequences - 5 and 6). Although the SD values are the same in Test Sequences - 3 and 4 created using 20x magnification objective, the RLI and AIS values of these sequences are different. Thus, it is proved that the magnification objective and the displayed specimen region affect the range scanned on the Z axis for the SFF approach.

Table 1. Test Sequences 1 - 6 created using different magnification objectives (10X - 20X - 40X) and displayed specimen regions

MO	Test Sequence	SD	RLI	ASI
10X	1	247.30	524	1047
	2	269.67	527	1053
20X	3	195.03	432	863
	4	204.80	432	863
40X	5	112.46	231	461
	6	108.57	222	443

3.3. Experiments for Definition of Ranges with Different Distances on the 2D Image Sequence

In the fourth step (Creating 2D Image Sequence with the Same Field of Perspective and Different Focused Regions in Optimal Range), the reference locations in the test sequences are centred and the Gaussian Distribution is adapted to the focus measures of the 2D images with the same field of perspective and different focused regions. As given in Table 2, the ranges with different distances (σ - 2σ - 3σ) on Test Sequences 1 - 6 are defined. For each test sequence (different magnification objective and the displayed specimen), the ranges (σ - 2σ - 3σ) with different amount of 2D images (AI), begin (BEGL) and end locations (ENL) are estimated. In addition, it is understood from the results in Table 2 that the amount of 2D images in the ranges decreases as the ratio of magnification objective increases from 10X to 40X.

Table 2. Ranges with different distances (σ - 2σ - 3σ) on Test Sequences 1 - 6

Test Sequence		σ	2σ	3σ	Test Sequence		σ	2σ	3σ
1	AI	248	494	742	2	AI	270	540	810
	BEGL	400	277	153		BEGL	392	257	122
	ENL	648	771	895		ENL	662	797	932
3	AI	196	390	596	4	AI	204	410	614
	BEGL	334	237	139		BEGL	330	227	125
	ENL	530	627	725		ENL	534	637	739
5	AI	112	224	338	6	AI	108	218	326
	BEGL	175	119	62		BEGL	168	113	59
	ENL	287	343	400		ENL	276	331	385

3.4. Experiments for Estimation of Optimal Range

Table 3. Quantitative results obtained from Quality Procedures of focus measurement operators for Test Sequence - 1

Focus Measurement Operator	σ		2σ		3σ		All 2D Images	
	SD	KM	SD	KM	SD	KM	SD	KM
Tenengrad [2]	**56.72**	**27.74**	72.69	28.07	153.6	30.24	229	31.79
Gradient Energy [5]	**55.84**	**26.11**	69.74	27.52	145.58	29.44	216.53	30.99
Multi-dir. Mod. Laplacian [9]	**25.44**	**11.43**	49.33	13.52	85.48	17.33	145.48	18.15
Modied Laplacian [10]	**53.75**	**25.55**	67.56	26.19	150.52	28.52	206.11	30.49
Variance [2]	**52.32**	**22.19**	65.31	24.01	145.16	27.33	200.56	29.59
DCT Energy Ratio [15]	**70.48**	**32.30**	90.48	36.48	180.03	40.45	250.48	45.01
3D Wavelet Transform [16]	**30.35**	**12.11**	52.15	13.33	85.52	16.99	142.55	19.03
Wavelet Coefficient Ratio [17]	**45.82**	**16.98**	60.73	19.45	88.44	22.01	146.09	24.47
Curvelet Coefficient Ratio [22]	**43.12**	**16.20**	58.09	19.06	88.66	21.47	149.32	23.84
3D Steerable Filters [24]	**42.15**	**14.48**	58.96	17.659	88.06	20.33	145.55	22.95

Table 4. Quantitative results obtained from Quality Procedures of focus measurement operators for Test Sequence - 2

Focus Measurement Operator	σ		2σ		3σ		All 2D Images	
	SD	KM	SD	KM	SD	KM	SD	KM
Tenengrad [2]	**57.06**	**29.48**	62.48	31.33	94.12	32.80	152.5	35.06
Gradient Energy [5]	**58.01**	**28.47**	64.09	29.37	88.25	33.82	158.69	36.40
Multi-dir. Mod. Laplacian [9]	**35.98**	**17.56**	50.44	18.45	80.13	21.12	139.72	23.90
Modied Laplacian [10]	**52.21**	**26.46**	56.12	28.58	100.15	30.01	146.12	31.98
Variance [2]	**53.44**	**23.14**	63.49	25.56	100.01	28.09	166.63	30.54
DCT Energy Ratio [15]	**75.98**	**38.44**	100.66	41.85	206.54	45.59	252.88	50.17
3D Wavelet Transform [16]	**40.16**	**18.81**	53.68	20.02	82.11	23.56	143.09	25.98
Wavelet Coefficient Ratio [17]	**42.10**	**19.56**	58.84	20.12	83.32	22.96	144.15	25.46
Curvelet Coefficient Ratio [22]	**44.88**	**19.98**	56.61	21.33	81.56	23.56	146.38	26.01
3D Steerable Filters [24]	**41.84**	**18.55**	57.32	20.95	82.09	21.48	145.68	25.60

Table 5. Quantitative results obtained from Quality Procedures of focus measurement operators for Test Sequence - 3

Focus Measurement Operator	σ		2σ		3σ		All 2D Images	
	SD	KM	SD	KM	SD	KM	SD	KM
Tenengrad [2]	**68.05**	**20.52**	79.26	25.89	101.98	30.98	148.52	40.03
Gradient Energy [5]	**69.63**	**19.35**	79.42	24.44	98.55	29.84	150.65	39.56
Multi-dir. Mod. Laplacian [9]	**42.50**	**9.53**	50.64	14.21	75.01	18.34	123.42	21.98
Modied Laplacian [10]	**64.23**	**21.10**	72.50	26.91	96.33	29.09	148.11	38.98
Variance [2]	**65.56**	**22.66**	71.11	24.63	98.95	29.12	161.55	39.65
DCT Energy Ratio [15]	**80.44**	**31.55**	101.14	38.11	170.35	43.84	231.69	48.33
3D Wavelet Transform [16]	**41.14**	**12.98**	51.98	17.50	83.37	19.25	138.91	21.43
Wavelet Coefficient Ratio [17]	**59.54**	**16.25**	68.33	20.04	91.47	22.63	146.15	25.61
Curvelet Coefficient Ratio [22]	**58.19**	**18.13**	69.42	20.32	85.66	22.42	141.57	24.88
3D Steerable Filters [24]	**59.99**	**16.11**	70.63	19.12	84.98	20.97	142.42	24.65

Table 6. Quantitative results obtained from Quality Procedures of focus measurement operators for Test Sequence - 4

Focus Measurement Operator	σ		2σ		3σ		All 2D Images	
	SD	KM	SD	KM	SD	KM	SD	KM
Tenengrad [2]	**26.42**	**57.88**	30.80	103.79	50.82	121.30	85.88	139.22
Gradient Energy [5]	**27.33**	**56.45**	30.98	100.15	52.01	123.65	83.10	139.66
Multi-dir. Mod. Laplacian [9]	**18.12**	**45.22**	24.03	72.09	45.13	89.12	64.29	109.13
Modied Laplacian [10]	**25.09**	**58.01**	31.15	102.91	51.31	121.02	82.09	138.02
Variance [2]	**27.12**	**60.99**	33.48	99.55	53.25	124.87	80.48	137.66
DCT Energy Ratio [15]	**35.48**	**85.42**	42.56	125.13	65.01	140.56	91.12	157.33

3D Wavelet Transform [16]	**20.14**	**42.48**	27.13	69.13	42.12	85.12	63.19	106.12
Wavelet Coefficient Ratio [17]	**21.45**	**41.13**	26.89	70.05	43.98	84.98	62.42	105.98
Curvelet Coefficient Ratio [22]	**20.99**	**42.01**	25.42	71.49	42.81	85.23	61.56	104.13
3D Steerable Filters [24]	**20.52**	**41.45**	25.99	71.99	43.01	86.08	63.41	104.96

Table 7. Quantitative results obtained from Quality Procedures of focus measurement operators for Test Sequence - 5

Focus Measurement Operator	**σ**		**2σ**		**3σ**		**All 2D Images**	
	SD	**KM**	**SD**	**KM**	**SD**	**KM**	**SD**	**KM**
Tenengrad [2]	**24.10**	**14.81**	48.61	26.65	73.11	30.93	97.33	34.37
Gradient Energy [5]	**25.48**	**15.42**	49.89	25.98	69.13	29.45	91.98	33.57
Multi-dir. Mod. Laplacian [9]	**20.13**	**9.99**	36.81	17.98	42.11	26.10	63.19	30.01
Modied Laplacian [10]	**24.42**	**16.11**	45.82	24.42	56.43	30.45	95.38	34.31
Variance [2]	**26.98**	**18.12**	41.83	26.54	65.97	31.98	95.49	35.96
DCT Energy Ratio [15]	**38.55**	**28.41**	55.71	36.96	85.98	40.45	110.42	42.48
3D Wavelet Transform [16]	**21.46**	**9.12**	35.96	16.17	43.71	25.63	65.78	32.10
Wavelet Coefficient Ratio [17]	**22.09**	**10.01**	36.47	17.42	44.09	25.66	64.99	31.00
Curvelet Coefficient Ratio [22]	**21.44**	**9.89**	35.96	16.96	44.74	25.42	65.06	31.96
3D Steerable Filters [24]	**22.09**	**9.97**	35.02	17.09	43.87	26.01	64.83	32.09

Table 8. Quantitative results obtained from Quality Procedures of focus measurement operators for Test Sequence - 8

Focus Measurement Operator	**σ**		**2σ**		**3σ**		**All 2D Images**	
	SD	**KM**	**SD**	**KM**	**SD**	**KM**	**SD**	**KM**
Tenengrad [2]	**31.84**	**14.04**	49.56	19.86	83.49	32.31	101.54	41.33
Gradient Energy [5]	**33.56**	**15.98**	48.12	21.06	80.36	33.66	95.42	43.48
Multi-dir. Mod. Laplacian [9]	**24.42**	**9.56**	44.22	13.52	70.65	24.40	83.12	32.10
Modied Laplacian [10]	**36.48**	**16.42**	51.12	20.56	79.97	32.30	92.33	40.66
Variance [2]	**38.66**	**15.96**	53.96	21.42	78.99	33.20	93.44	41.42
DCT Energy Ratio [15]	**48.12**	**24.48**	60.44	36.54	95.12	46.10	100.66	55.57
3D Wavelet Transform [16]	**23.12**	**12.41**	42.10	15.65	72.66	25.60	85.12	33.48
Wavelet Coefficient Ratio [17]	**24.09**	**10.99**	41.55	14.99	71.96	23.47	84.44	32.77
Curvelet Coefficient Ratio [22]	**23.52**	**11.63**	40.97	14.66	72.48	23.66	83.66	31.55
3D Steerable Filters [24]	**23.66**	**11.48**	41.66	13.42	71.87	24.48	83.96	32.98

In order to estimate the optimal range, the second (computing focus measures) and third (selecting pixel with maximum focus degree) phases of our SFF approach described in Section 2 are implemented into the all ranges (σ - 2σ - 3σ) of the test sequences defined in the previous step. In the second (computing focus measures) phase, ten focus measurement operators (Tenengrad [2], Gradient Energy [5], Multidirectional Modified Laplacian [9], Modified Laplacian [10], Variance [2], DCT Energy Ratio [15], 3D Wavelet Transform [16], Wavelet Coefficient Ratio [17], Curvelet Coefficient Ratio [22], 3D Steerable Filters [24]) selected from different six subgroups are applied to all ranges to calculate the focusing information of the pixels. At the end of these phases, a total of 40 3D images are created for each test sequences.

The 3D image, which is considered to be a ground - truth in light microscopic systems, cannot created. Therefore, quality procedures that do not require a ground - truth are used in order to estimate the optimal range for SFF approaches. These quality procedures are Standard Deviation (SD) and Kurtosis Metric (KM).

Quantitative results obtained the quality procedures of focus measurement operators for all test sequences are shown in Tables 3 - 8. As mentioned in the previous sections, it is expected that the 3D image produced by using a sequence consisting of 2D images in the optimal range have lower variations and outliers (lower KM and SD values). For estimation of optimal range, a total of 40 3D images for each test sequence are evaluated based on their variations and outliers. It is obvious in the results of the quality procedures of focus measurement operators for all test sequences that the variation and outliers in the 3D images vary with the magnification objectives and ranges. As the range expands from σ to 3σ, the KM and SD values of the 3D images for each test sequence increase. The 3D images created with 2D images in the range (σ) have the values of variations and outliers. With qualitative results, it is determined that optimum range is (σ) in each magnification objective for SFF approaches.

Fig. 4 shows 3D images created using Curvelet Coefficient Ratio with 2D images with the same field of perspective and different focused regions in (a) (σ), (b) (2σ), (c) (3σ) and (d)

all ranges of Test sequences - 6. Subjective evaluation of the visual results indicates that 3D images created using 2D images with the same field of perspective and different focused regions in the range (σ) have fewer outliers than the others. Thus, it is proven that quantitative results are in accord with visual results.

Conclusion

In this paper, a novel SFF approach is improved to reconstruct the specimen's 3D image with lower outliers and variations for cytopathological examination. The suggested SFF approach consists of three primary phases; (1) estimation of optimal range, (2) computing focus measures and (3) selecting pixel with maximum focus degree. In the first phase of well-known SFF approaches, a sequence consisting of the 2D images with the same field of

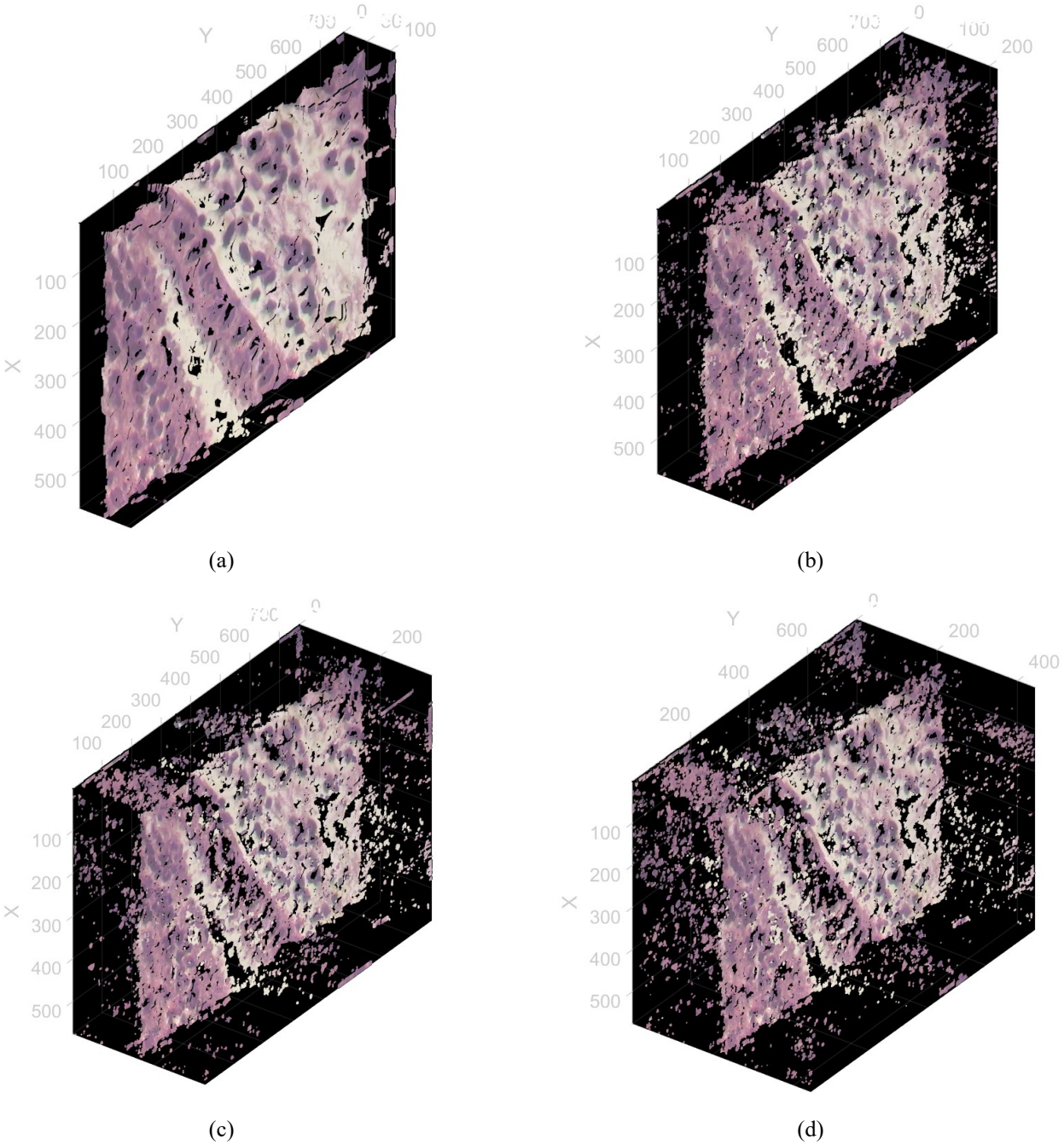

Fig. 4. 3D images created using Curvelet Coefficient Ratio with 2D images with the same field of perspective and different focused regions in (a) (σ), (b) (2σ), (c) (3σ) and (d) all ranges of Test Sequence - 6.

perspective and different focused regions are generated by moving the microscope platform along the specified range. This range is randomly defined between the begin and end locations on the Z axis. In order to produce the specimen's 3D image with more prominent knowledge and details and to scan the entire 3D structure of the specimen on the Z axis, the proposed research estimates optimal range between the begin and end locations. The complete amount of 2D images with the same field of perspective and different focused regions, which is a critical factor influencing SFF

implementation on the microscopic system, is optimized in this research regardless of the type of the examined specimen and magnification objective. For both theoretical and practical analysis of our suggested approach, data sets consisting of real microscope image sequences are tested. A novel motorized microscope system that can provide auto - focusing and auto - scanning along the X - Y - Z axes is realized to acquire the real microscope image sequences.

In order to identify which range can transfer more significant information from the 2D images with the same field of perspective and different focused regions, quality procedures with non - requiring a ground-truth 3D image are preferred, which are SD and KM. It is expected that 3D images created with an optimal range give lower SD and KM values. In terms of the objective results obtained from the quality procedures for the test sequences, it is clearly seen that the efficiency of our suggested approach with the lowest values of SD and KM is superior to the other approaches.

Acknowledgements

This work has been supported by the TUBITAK Research Project 117E961.

References

[1] B. Billiot, F. Cointault, L. Journaux, J. C. Simon, P. Gouton, "3D Image Acquisition System Based on Shape from Focus Technique", Sensors, Vol. 13, No. 4, pp. 5040-5053, 2013.

[2] S. Pertuz, D. Puig, M A. Garcia, "Analysis of focus measure operators for shape-from-focus", Pattern Recognition, Vol. 46, No. 5, pp. 1415-1432, 2013.

[3] S. O. Shim, A. S. Malik, T. S. Choi, "Accurate shape from focus based on focus adjustment in optical microscopy", Microscopy Research and Technique, Vol. 72, No. 5, pp. 362-370, 2009.

[4] J. M. Geusebroek, F. Cornelissen, A. W. Smeulders, H. Geerts, "Robust autofocusing in microscopy", Cytometry: The Journal of the International Society for Analytical Cytology, Vol. 39, No. 1, pp. 1-9, 2000.

[5] A. S. Malik, T. S. Choi, "A novel algorithm for estimation of depth map using image focus for 3d shape recovery in the presence of noise", Pattern Recognition, Vol. 41, No. 7, pp. 2200-2225, 2008.

[6] M. B. Ahmad, T. S. Choi, "Application of three dimensional shape from image focus in lcd/tft displays manufacturing", IEEE Transactions on Consumer Electronics, Vol. 53, No. 1, pp. 1-4, 2007.

[7] Y. An, G. Kang, I. J. Kim, H. S. Chung, J. Park, "Shape from focus through laplacian using 3d window", Second International Conference on Future Generation Communication and Networking, pp. 46-50, December 2008.

[8] J. L. Pech Pacheco, G. Cristobal, J. Chamorro Martinez, J. Fernandez Valdivia, "Diatom autofocusing in brightfield microscopy: a comparative study", Proceedings 15th International Conference on Pattern Recognition, pp. 314-317, 2000.

[9] T. Yan, Z. Hu, Y. Qian, Z. Qiao, L. Zhang, "3D shape reconstruction from multifocus image fusion using a multidirectional modified Laplacian operator", Pattern Recognition, Vol. 98, 107065, 2020.

[10] S. Nayar, Y. Nakagawa, "Shape from focus: an effective approach for rough surfaces", IEEE International Conference on Robotics and Automation, 1990, pp. 218-225, 1990.

[11] C. Y. Wee, R. Paramesran, "Measure of image sharpness using eigenvalues", Information Sciences, Vol. 177, No. 12, pp. 2533-2552, 2007.

[12] P. T. Yap, P. Raveendran, "Image focus measure based on chebyshev moments", IEE Proceedings-Vision, Image and Signal Processing, Vol. 151, No. 2, pp. 128-136, 2004.

[13] S. Y. Lee, Y. Kumar, J. M. Cho, S. W. Lee, S. W. Kim, "Enhanced autofocus algorithm using robust focus measure and fuzzy reasoning", IEEE Transactions on Circuits and Systems for Video Technology, Vol. 18, No. 9, pp. 1237-1246, 2008.

[14] S. Y. Lee, J. T. Yoo, Y. Kumar, S. W. Kim, "Reduced energy-ratio measure for robust autofocusing in digital camera", IEEE Signal Processing Letters, Vol. 16, No. 2, pp. 133-136, 2009.

[15] C. H. Shen, H H., Chen, "Robust focus measure for low-contrast images", Digest of Technical Papers International Conference on Consumer Electronics, pp. 69-70, 2006.

[16] U. Ali, M. T. Mahmood, "3d shape recovery by aggregating 3d wavelet transform-based image focus volumes through 3d weighted least squares", Journal of Mathematical Imaging and Vision, Vol. 62, No. 1, pp. 1-19, 2019.

[17] H. Xie, W. Rong, L. Sun, "Wavelet-based focus measure and 3-d surface reconstruction method for microscopy images", IEEE/RSJ International Conference on Intelligent Robots and Systems. pp. 229-234, 2006.

[18] F. S. Helmli, S. Scherer, "Adaptive shape from focus with an error estimation in light microscopy", Image and Signal Processing and Analysis, pp. 188-193, 2001.

[19] M. V. Shirvaikar, "An optimal measure for camera focus and exposure", Proceedings of the Thirty-Sixth South eastern Symposium, pp. 472-475, 2004.

[20] H. Nanda, R. Cutler, "Practical calibrations for a real-time digital omnidirectional camera", CVPR Technical Sketch, Vol. 20, No. 2, 2001.

[21] J. Lorenzo, M. Castrillon, J. Mendez, O. Deniz, "Exploring the use of local binary patterns as focus measure", Computational Intelligence for Modelling Control Automation, pp. 855-860, 2008.

[22] R. Minhas, A. Adeel Mohammed, M. Q. Jonathan Wu, "Shape from focus using fast discrete curvelet transform", Pattern, Recognition, Vol. 44, No. 4, pp. 839-853, 2011.

[23] F. Mahmood, J. Mahmood, A. Zeb, J. Iqbal, "3d shape recovery from image focus using gabor features", Tenth International Conference on Machine Vision, 2017.

[24] T. Fan, H. Yu, "A novel shape from focus method based on 3d steerable Filters for improved performance on treating textureless region", Optics Communications, Vol. 410, pp. 254-261, 2018.

[25] S. Pertuz, D. Puig, M. A. Garcia, "Reliability measure for shape-from-focus", Image and Vision Computing, Vol. 31, No. 10, pp. 725-734, 2013.

[26] I. Lee, M. T. Mahmood, T. S. Choi, "Adaptive window selection for 3D shape recovery from image focus", Optics Laser Technology, Vol. 45, pp. 21-31, 2013.

[27] M. Muhammad, T. S. Choi, "Sampling for shape from focus in optical microscopy", IEEE Transactions on Pattern Analysis and Machine Intelligence, Vol. 34, No. 3, pp. 564-573, 2012.

[28] C. Y. Tseng, S. J. Wang, "Shape-from-focus depth reconstruction with a spatial consistency model", IEEE Transactions on Circuits and Systems for Video Technology, Vol. 24, No. 12, pp. 2063-2076, 2014.

[29] W. Liu, X. W. Key, "Semi-global depth from focus", 3rd IAPR Asian Conference on Pattern Recognition (ACPR), pp. 624-629, 2015.

[30] D. C. Tsai, H. H. Chen, "Focus profile modeling", IEEE Transactions on Image Processing, Vol. 25, No. 2, pp. 818-828, 2016.

[31] M. J. Muhammad, T. S. Choi, "Sampling for shape from focus in optical microscopy", IEEE Transactions on Pattern Analysis and Machine Intelligence, Vol. 34, No. 3, pp. 564-573, 2012.